PCCP

CrossMark
click for updates

Phase-modulated electronic wave packet interferometry reveals high resolution spectra of free Rb atoms and Rb*He molecules

Lukas Bruder,* Marcel Mudrich and Frank Stienkemeier

Phase-modulated wave packet interferometry is combined with mass-resolved photoion detection to investigate rubidium atoms attached to helium nanodroplets in a molecular beam experiment. The spectra of atomic Rb electronic states show a vastly enhanced sensitivity and spectral resolution when compared to conventional pump–probe wave packet interferometry. Furthermore, the formation of Rb*He exciplex molecules is probed and for the first time a fully resolved vibrational spectrum for transitions between the lowest excited $5\Pi_{3/2}$ and the high-lying electronic states $2^2\Pi$, $4^2\Delta$, $6^2\Sigma$ is obtained and compared to theory. The feasibility of applying coherent multidimensional spectroscopy to dilute cold gas phase samples is demonstrated in these experiments.

1 Introduction

Wave packet interferometry (WPI) is a fundamental and versatile tool to study and control the quantum dynamics in a wide range of target systems.[1–6] In these experiments, two wave packets (WPs) prepared by identical but temporally separated optical pulses interfere constructively or destructively depending on their relative phase. The observation of such interferences is the prerequisite in coherent time-resolved spectroscopy or coherent control experiments.[1,2] The success of this technique usually relies on the precise control of the relative phase between pump and probe pulses and phase stabilization methods are required if a complete description of the coupled electronic and nuclear dynamics is desired.[2]

Likewise, precise phase control is a key issue in higher order schemes such as optical multidimensional spectroscopy.[7] Several phase stabilization methods have been developed[8–19] to make two-dimensional electronic spectroscopy (2DES) accessible to the visible[20] and ultraviolet optical range.[21] 2DES has been applied to systems ranging from atomic vapors[10,15] to complex molecular systems in the liquid phase[22,23] and bulk semiconductor nanostructures.[24] However, complementary investigations of dilute cold targets in molecular beams are yet missing.

Recently, the Marcus group has established a collinear passively phase-stabilized 2DES scheme based on continuous acousto-optic phase modulation combined with lock-in demodulation (PM2D spectroscopy).[15] A variant of this technique has been implemented by the Cundiff group.[17] PM2D spectroscopy

has been combined with fluorescence and photocurrent detection[15,17,25] and the applicability to highly dilute solutions was demonstrated.[26] The signal recovery capabilities of lock-in amplification and the incorporation of incoherent observables make this approach an ideal candidate for single-molecule or molecular beam studies. Initially, the phase modulation (PM) technique was demonstrated in a WPI experiment of atomic Rb vapor using fluorescence detection (PM-WPI).[27] In the current work, we combine this PM-WPI scheme with mass-resolved photoion detection to investigate a dilute molecular sample in a supersonic beam setup.

Helium nanodroplet isolation has been established as a unique technique for spectroscopic studies at millikelvin temperatures.[28–30] Atoms, molecules as well as complexes or clusters can be isolated in a weakly perturbing helium environment providing an ideal matrix where the spectroscopic resolution is significantly improved; not only in comparison with experiments in room temperature solvents,[31,32] but also when compared to other cryogenic matrices or clusters.[33] Time-resolved experiments using femtosecond (fs) lasers[34] have focused on various photodynamical processes of doped He droplets. These include vibrational WP propagation,[35,36] complex formation,[37,38] fragmentation dynamics,[34] desorption[39,40] and various aspects of energy dissipation and decoherence.[41,42]

Alkali metal atoms and small complexes, which are weakly bound at the surface of the droplets, were among the first species to be studied by electronic spectroscopy in He droplets.[43] Upon excitation to the lowest excited P state, the enhanced interaction with helium leads to the formation of alkali–helium exciplex molecules which desorb off the droplet and can be probed in the gas phase.[5,37,38,44,45] The formation dynamics has been discussed

Physikalisches Institut, Universität Freiburg, 79104 Freiburg, Germany.
E-mail: lukas.bruder@physik.uni-freiburg.de

This journal is © the Owner Societies 2015

Phys. Chem. Chem. Phys., 2015, **17**, 23877–23885 | 23877

for different alkali exciplexes (Na*He, K*He, and Rb*He).[38,44–47] Moreover, comparative studies using He droplets formed with the fermionic isotope [3]He have been performed in order to probe the influence of superfluidity of the droplets.[37]

WPI experiments for the first time enabled us to access the vibrational energies of such unstable complexes.[5] However, since only differences between individual vibrational levels are accessible using this technique, the assignment of vibrational states could not been done rigorously, and in particular the role of higher-lying electronic states correlating with the 5D atomic asymptote has not been included. Later, femtosecond pump–picosecond probe experiments have probed the dynamics of individual vibronic levels.[38] These measurements confirmed the previous rough assignment; however the spectral resolution stayed behind the one achieved using the WPI technique. In the current work, we present a new experimental approach to study the vibronic structure of cold isolated molecular samples by PM-WPI using photoion detection. The new PM technique provides both a direct access of vibronic energies and a vastly enhanced spectral resolution, which allows us to determine a large number of contributing states. In this way the involved potentials can be accurately tested on a level beyond that of current *ab initio* calculations.

2 He droplet beam generation and exciplex formation

The molecular beam apparatus comprises of a differentially pumped vacuum system where the formation of droplets, doping of droplets, and laser interaction and detection are individually housed and separated by gate valves (Fig. 1). The droplets are formed in a continuous flow supersonic expansion from a nozzle of 5 μm in diameter, attached to a closed cycle refrigerator. The expansion conditions are: nozzle temperature $T_0 = 17$ K and backing pressure $p_0 = 50$ bar, which corresponds to a mean cluster size of He_N, $N = 20\,000$.[34] Doping of the He droplets with Rb atoms is achieved in a heated vapor cell which is stabilized to a temperature $T_{Rb} = 358$ K. At this temperature, the Rb vapor pressure is such that on average only one Rb atom is attached to each droplet. The fs laser pulses intersect the doped droplet beam perpendicularly inside the ion extraction region of a commercial quadrupole mass spectrometer (QMS). Since atoms and exciplexes tend to desorb off the droplets upon electronic
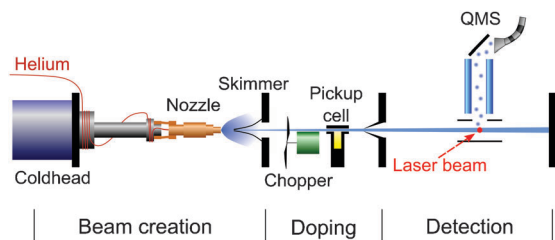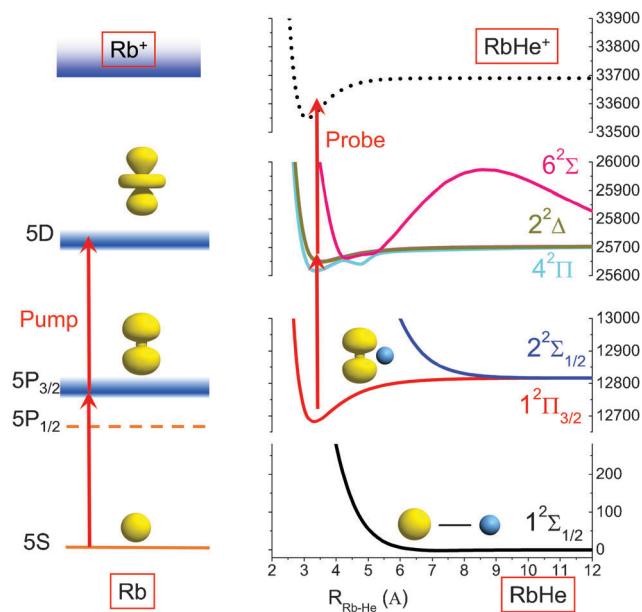

Fig. 2 Pump–probe excitation scheme. The Rb $5P_{3/2}$ and 5D states are coherently excited. The broadening of states induced by the helium environment is indicated. The relevant Rb*He pair potentials of the formed exciplexes and the probe process are illustrated in the right panel.

excitation,[40] the photo-ionized atoms and exciplexes are detected in the gas phase. Rb and Rb*He ions are resolved well separated from each other in the mass spectrum.

The formation of Rb*He molecules is based on the attractive interaction of Rb excited states with He atoms, mainly due to a missing Pauli repulsion in the nodal region of extended electron orbitals having an angular momentum of $l > 0$. However, a complete understanding of the formation and desorption process of metal–He exciplexes at He droplets is still missing. Different models have been discussed in order to interpret the formation of alkali–helium exciplexes and the measured time dependent signals. Tunneling processes have been modeled[48–51] and direct laser-excitation of bound states in the excited pair potential has been discussed.[39,47,52,53] In Fig. 2 the potentials of the relevant states for our experiment are plotted and the pump–probe scheme is illustrated by vertical arrows.

3 Phase-modulated wave packet interferometry

Conventional pump–probe spectroscopy allows us to follow the population dynamics in a quantum system at real-time, however not the dynamics of coherences or coupled electronic-vibrational dynamics. (Electronic) WPI experiments, on the contrary, give access to the full information content by employing a coherent excitation scheme involving phase-related pump–probe pulses.[2] In this approach, two WPs separately excited by pump and probe pulses interfere with each other, giving rise to constructive and destructive interference effects in the underlying quantum system. In the regime of weak optical perturbation, WPI is equivalent to quantum beat measurements,

Fig. 1 Schematic illustration of the molecular beam machine. A helium cluster beam traverses differentially pumped vacuum chambers housing the droplet source, pick-up cell and detector, respectively.

23878 | *Phys. Chem. Chem. Phys.,* 2015, **17**, 23877–23885

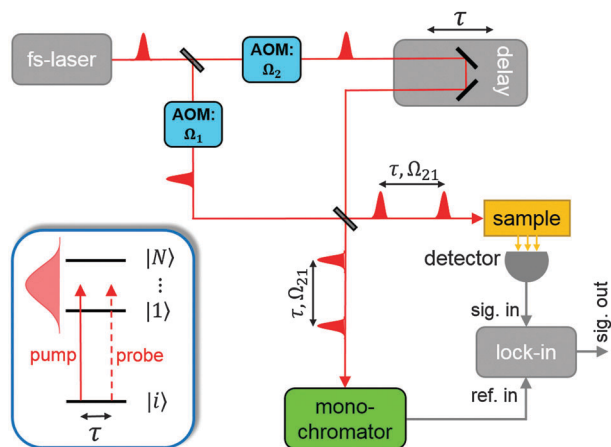This journal is © the Owner Societies 2015

Fig. 3 Simplified diagram of the PM-WPI scheme. Fs pump–probe pulse sequences are generated using a Mach–Zehnder interferometer. AOMs impart a continuous phase-modulation onto the optical pulses. A monochromator is used to construct a reference signal for lock-in demodulation of the acquired WPI data. The box labeled sample represents the molecular beam machine. The inset shows the generalized WPI excitation scheme.

Ramsey fringes in the time domain,[54,55] Fourier spectroscopy using fs pulses,[56] or temporal coherent control.[57]

In more detail, we consider a simple system consisting of a few discrete energy eigenstates $|i\rangle,|1\rangle,\ldots,|N\rangle$ as shown in the inset of Fig. 3. The pump pulse excites a coherent superposition of the initial state $|i\rangle$ and excited states $|n\rangle$ lying within the laser bandwidth. This WP evolves freely in time until the probe pulse excites a second WP. The interference of the two WPs induces a modulation of the excited state populations with respect to the pump–probe delay τ. Probing the excited state populations while systematically scanning τ yields a typical quantum beat signal[58]

$$S(\tau) = \sum_{n=1}^{N} A_n[1 + \beta\cos(\omega_{ni}\tau)], \quad (1)$$

where $\omega_{ni} = (E_n - E_i)/\hbar$ corresponds to the energy differences of the optical transitions from level $|i\rangle$ into $|n\rangle$. $A_n \propto |D_{ni}|^2\tilde{E}^2(\omega_{ni})$ represents the transition probability for each $|n\rangle \leftarrow |i\rangle$ transition, where $\tilde{E}(\omega)$ is the Fourier transform of the single pulse electric field (assuming identical pump and probe pulses) and D_{ni} represents the transition dipole moment of the relevant degrees of freedom (electronic, vibrational and rotational). For simplicity, a temporal overlap between pump and probe pulses is neglected and their relative carrier-envelope phase is set to zero. The constant part in eqn (1) originates from excitation pathways involving interactions with pump or probe pulses only and thus does not depend on the pump–probe delay, whereas the oscillating part reflects the WP interference. The dimensionless parameter $\beta \leq 1$ determines the contrast of the quantum beat signal. Theoretically, it is $\beta = 1$, however, the experimental conditions (mainly optical alignment and the probing mechanism) often drastically reduce the quantum beat contrast.

The PM-WPI approach of the Marcus group effectively extracts the pure WP interference contribution of eqn (1) by combining acousto-optic PM with lock-in demodulation. A detailed description of the PM-WPI scheme is given by Tekavec et al.[27] We apply this technique in an almost identical optical setup (schematically shown in Fig. 3). Briefly, pump–probe pulse pairs of adjustable delay are generated in a Mach–Zehnder type interferometer and are collinearly superimposed afterwards. An acousto-optic modulator (AOM) is placed in each branch of the interferometer, which shifts the carrier frequency of pump and probe pulses individually by the applied acoustic frequencies, denoted $\Omega_j, j = 1, 2$. Phase-locked driving of the two AOMs thus imparts a well-defined difference frequency $\Omega_{21} = \Omega_2 - \Omega_1$ onto the two-pulse intensity function of the copropagating pulses. In principle, this is equivalent to shot-to-shot phase-cycling, where the relative phase between pump and probe pulses is incremented by $\Delta\phi = \Omega_{21}/\nu_{rep}$ (ν_{rep} being the laser repetition rate) between each laser shot.[17] Eventually, this results in excited state populations in the sample that exhibit, besides the typical quantum beat of eqn (1), an additional continuous modulation with the difference frequency of the AOMs

$$S_{in}(\tau, t) = \sum_{n=1}^{N} A_n[1 + \beta\cos(\omega_{ni}\tau - \Omega_{21}t)]. \quad (2)$$

In our experiments, it is $\nu_{rep} = 80$ MHz and $\Omega_{21} = 5$ kHz. Hence, Ω_{21} is quasi-continuously sampled and t can be regarded as a continuous time variable. The two-pulse intensity function is spectrally filtered using a monochromator in a separate beam, yielding a reference signal for phase-synchronous detection,

$$R(\tau, t) = R_0[1 + \cos(\omega_M\tau - \Omega_{21}t)]. \quad (3)$$

Here the band-pass filter function of the monochromator is centered at the frequency denoted ω_M. Applying the signal of eqn (2) to a lock-in amplifier while referencing the device with the signal of eqn (3) results in an output signal of the form

$$S_{out}(\tau) = \sum_{n=1}^{N} A_n\beta\cos[(\omega_{ni} - \omega_M)\tau]. \quad (4)$$

It is straightforward to apply these considerations to target systems of different energetic structures. In the current work, we investigate atomic Rb as well as Rb*He exciplex molecules by means of photoionization and subsequent mass-resolved ion detection. In the atomic case, we follow excitation pathways where coherent superpositions of the $5S_{1/2}$ and $5P_{3/2}$ states as well as of the $5P_{3/2}$ and $5D_{5/2,3/2}$ states are induced, as indicated in Fig. 2. In the molecular case, we prepare coherent superpositions between the vibrational states of the potential energy curves (PECs) correlating with the $5P_{3/2}$ and $5D_{5/2,3/2}$ asymptotic atomic states, also indicated in Fig. 2. In both cases, the phase-related pump–probe sequence eventually prepares a stationary population state in the target system which is ionized by subsequent absorption of additional photons within the same probe pulse or by consecutive pulses. In analogy to fluorescence detection,[27] the ion yield reflects the mean population probability of the excited

This journal is © the Owner Societies 2015

Phys. Chem. Chem. Phys., 2015, 17, 23877–23885 | 23879

states and is thus directly proportional to the individual beat components of eqn (4).

When comparing the outcome of a conventional WPI experiment (eqn (1)) with the outcome of a PM-WPI experiment (eqn (4)), several advantages of the latter method become obvious. In PM-WPI experiments, one measures the actual optical transition frequencies relative to the monochromator frequency, resulting in a strongly undersampled quantum beat signal. Therefore, the same information content can be inferred from a much smaller amount of sampling points. Moreover a time-delay jitter due to mechanical instabilities within the interferometer scales to a significantly less extent and the laboratory noise in general is strongly suppressed by the lock-in demodulation process. As mentioned above, the phase modulation scheme introduces shot-to-shot or dynamic phase-cycling.[17] As a consequence, only pathways which imprint an Ω_{21}-modulation in the final population state are extracted, resulting in a post-selection of all optically induced excitation pathways. In this way, solely contributions from electronic WP interference are detected, whereas contributions originating, for instance, from pure vibrational WPs are removed from the signal. More details about post-selection by phase-cycling can be found in ref. 58.

For the PM-WPI optical setup we employ a titanium:sapphire oscillator producing pulses of about 200 fs duration and 70 cm^{-1} spectral width (FWHM) at a repetition rate of 80 MHz. The average laser power is about 2 W at the laser exit window, leading to pulse energies of 1.7 nJ (pump) and 5.2 nJ (probe) before entering the vacuum apparatus. The laser beam is focused using a lens of 150 mm focal length, resulting in a beam diameter of 40 μm at the interaction volume. For the presented atomic Rb measurements, the monochromator is set to 12897.78 cm^{-1} and time domain interferograms are acquired by sampling the pump–probe delay in 30 fs steps from 0 to 50 ps while 1000 data points are averaged for each delay position. For the Rb*He exciplex measurements, the monochromator is set to 12904.15 cm^{-1}, the pump–probe delay is scanned from −100 to 120 ps in increments of 50 fs and 1500 data points are averaged for each delay position. The QMS signal is amplified before feeding it into the lock-in amplifier. The monochromator signal is acquired using an avalanche photo diode, band-pass filtered and amplified. Signal demodulation is done with a lock-in time constant of 30 ms and 18 dB roll-off. Demodulated in-phase (X) and in-quadrature (Y) signals are acquired simultaneously to reconstruct the complex-valued amplitude $Z = X + iY$. A discrete Fourier transform of Z is performed after applying a Gaussian window function and zero-padding. The frequency axis of the obtained spectrum is shifted by the amount of the monochromator frequency in order to reconstruct the absolute transition frequencies. In the case of exciplex experiments, the frequency spectrum is additionally deconvoluted with the pump–probe autocorrelation function, analogous to the procedure applied in ref. 59.

4 PM–WPI of atomic Rb attached to He droplets

To demonstrate the advantages of the PM method, we show at first measurements of atomic Rb attached to He droplets,
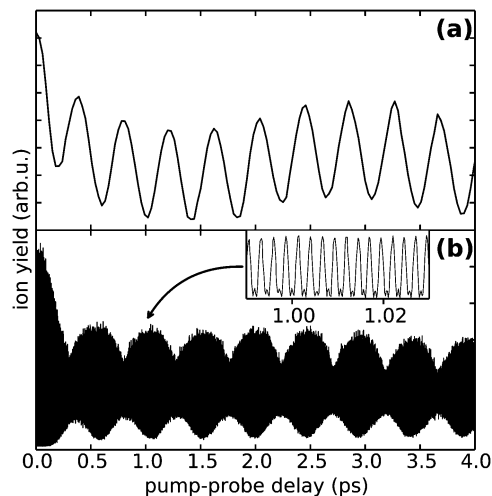

Fig. 4 WPI measurements of Rb atoms attached to He droplets. (a) Shows the Rb ion yield as a function of pump–probe delay obtained from a PM-WPI measurement (in-phase component) and (b) respective data obtained in a conventional WPI experiment. Comparing the signal frequencies in (a) with the inset of (b) highlights the drastic frequency downshifting effect inherent in the PM-WPI technique.

which serves as a simple model system with only four electronic states involved, as illustrated in Fig. 2. For this purpose the mass spectrometer is tuned to the mass of the most abundant isotope ^{85}Rb and the laser wavelength is set to 775 nm. The $5S_{1/2} \rightarrow 5P_{3/2}$ and $5P_{3/2} \rightarrow 5D_{5/2,3/2}$ transitions are separated by 70.40 cm^{-1} and 67.44 cm^{-1}, respectively, which fall into the bandwidth of the fs pulses. In the applied WPI scheme, interference among pump and probe excitation thus results in excited state populations that exhibit delay-dependent oscillations corresponding to the mentioned optical transition frequencies. We compare the PM-WPI data with conventional WPI measurements previously conducted in our group using the same equipment, under similar experimental conditions.[60] Fig. 4 shows the ion yield for the first 4 ps of the pump–probe delay for the PM-WPI (a) and conventional WPI case (b), respectively. Both interferograms exhibit an exaggeration of the ion yield around zero delay resulting from the temporal overlap of pump and probe pulses. Fig. 5 shows the discrete Fourier transforms of the time domain data. The pronounced peaks in (a) correspond precisely to the expected $5S_{1/2} \rightarrow 5P_{3/2}$ and $5P_{3/2} \rightarrow 5D_{5/2,3/2}$ transitions (shown as gray dashed lines). Here even the spin–orbit splitting of the 5D state ($\Delta = 2.96$ cm^{-1}) is resolved, whereas in (b) transition frequencies can be identified only qualitatively and the splitting of the 5D state is not resolved.

Two effects are responsible for the drastic difference in signal quality achieved by the two experimental techniques. On the one hand, the PM-WPI data are measured in the rotating frame defined by the monochromator frequency, which results in strong undersampling of the quantum beat frequencies. In the conventional WPI experiment (Fig. 4(b)) the optical transition frequencies are fully sampled as shown in the inset, whereas in Fig. 4(a) the pump–probe transients are measured in
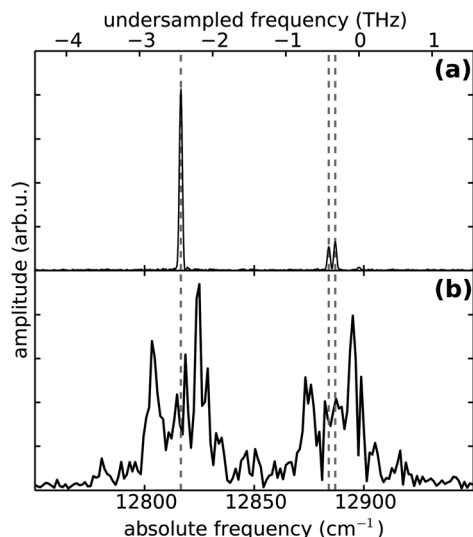
23880 | Phys. Chem. Chem. Phys., 2015, 17, 23877–23885

This journal is © the Owner Societies 2015

Fig. 5 Discrete Fourier transform of the PM-WPI time domain data (a) and conventional WPI data (b), respectively, for measurements of Rb atoms attached to He droplets. The absolute frequencies given by the bottom scale are common for both graphs. The scale at the top shows the downshifted frequencies at which the pump–probe transient is detected in the PM scheme before being shifted by the monochromator frequency. Vertical dashed lines indicate the atomic Rb transition frequencies.

the rotating frame and thus downshifted from ≈ 380 THz to below 3 THz (refer to the top frequency scale in Fig. 5). This significantly reduces the demands on phase stability in the optical setup. In the presented conventional WPI experiment, phase errors have been partially compensated by tracking the interferogram of a HeNe laser while scanning the pump–probe delay whereas no phase corrections have been applied in the PM scheme. Nonetheless, the latter case exhibits a drastic improvement in resolution and an excellent signal-to-noise ratio. At the same time, less data points are required to obtain the same information: the PM-WPI data set (0–50 ps pump–probe delay, 50 fs step size) comprises only 1.6% of the sampling points acquired in the fully sampled case (0–63 ps pump–probe delay, 0.6 fs step size).

On the other hand, imprinting a well-defined modulation onto the WPI signal allows utilizing efficient lock-in detection to extract weak signals from very large background contributions. This advantage of the PM method is particularly important when investigating highly dilute samples. In He droplet beam experiments, target densities are estimated to fall below 10^8 cm^{-3}[34] which usually puts a severe constraint on the achievable signal-to-noise ratio; the lock-in amplification in the PM scheme, however, provides great background suppression.

5 PM-WPI of Rb*He exciplexes

5.1 Experimental results

After having established the accuracy and sensitivity of the PM-WPI method, we turn towards studying Rb*He exciplexes, the spectra of which have not yet been recorded with high resolution. PM-WPI measurements are conducted by tuning the

mass spectrometer to 89 amu and the laser wavelength to 774 nm. Signal strengths are a factor of 20 smaller than in the atomic Rb case. In the PM-WPI scheme, vibronic transitions between the $1^2\Pi_{3/2}$ potential energy curve (PEC) correlating with the $5P_{3/2}$ and the $2^2\Pi$, $4^2\Delta$, $6^2\Sigma$ PECs correlating with the $5D_{5/2,3/2}$ atomic Rb states are probed (cf. Fig. 2). Pure vibrational transitions within the same PEC or transitions among the $2^2\Pi$, $4^2\Delta$, $6^2\Sigma$ PECs are not detected due to the above mentioned post-selection of signal contributions within the phase-cycling procedure.

A Fourier transform of the pump–probe transient yields a fully resolved vibrational spectrum of the exciplex molecule (Fig. 6) with a spectral resolution of 0.3 cm^{-1} (FWHM). Comparing the spectral lines with the position of the $5P_{3/2} \rightarrow 5D_{5/2,3/2}$ atomic Rb transitions (black dashed lines), an intuitive interpretation is possible: the closely spaced spectral lines in the vicinity of the atomic transitions involve mainly vibrational modes energetically close to the dissociation limits. Lines at larger frequencies correspond to transitions of lower lying vibrational modes in the $1^2\Pi_{3/2}$ electronic state and the line splitting originates from the congestion of the higher-lying PECs.

Let us compare our data with previous photoionization studies of the Rb*He exciplex. In a conventional WPI experiment[5] the signal quality was not sufficient to deduce the absolute transition frequencies through a direct Fourier analysis; relative distances between vibrational levels were deduced instead. To compare with our PM-WPI results, we assign the relative frequencies obtained in ref. 5 to the distances between spectral features in our study (Fig. 6, blue scale on top). We find good agreement albeit our spectrum exhibits a factor 10 better resolution and allows a more unambiguous interpretation. A different approach for achieving vibrationally resolved data on Rb*He exciplex molecules has been pursued in a femtosecond pump–picosecond probe experiment.[38] This study
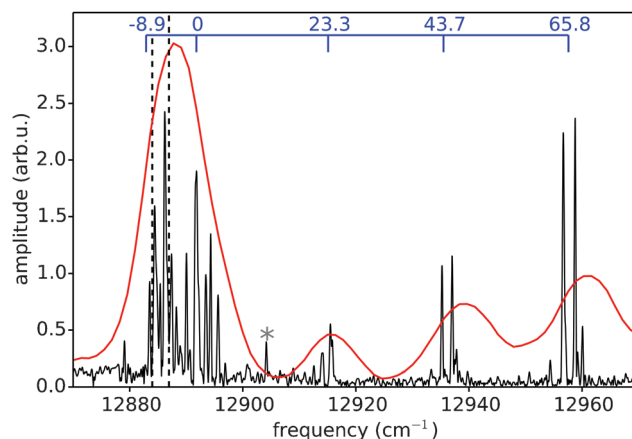

Fig. 6 Rb*He exciplex spectrum obtained from PM-WPI (black) and fs pump ps probe (red) measurements.[38] Relative transition frequencies inferred from conventional WPI[5] are also shown (blue scale on top). Black dashed lines indicate the $5P_{3/2} \rightarrow 5D_{5/2,3/2}$ atomic Rb transitions. In the PM-WPI spectrum, one peak originating from the laboratory noise appears at the employed monochromator frequency (asterisk).

provided absolute transition frequencies although at the cost of resolution which is factor 30 lower than that achieved in our measurement. After applying a red shift of 2 cm^{-1} to the corresponding data (red spectrum in Fig. 6) good agreement with our spectrum is obtained despite the different measurement schemes. The systematic shift can be attributed to coarse calibration of the pulse shaper that was used to generate the ps probe pulses. Calibration errors in the PM-WPI data can be excluded since calibration measurements with a Rb vapor cell have been carried out regularly during the measurements.

Previously, two types of dynamics have been observed when forming Rb*He exciplexes on the surface of He droplets. On the one hand, a fast process on the few ps timescale is observed[5] which can be attributed to an impulsive response of the He droplet environment to the electronic excitation of the Rb atom. On the other hand, slow relaxation of vibrational modes on the ns timescale is observed and attributed to slow vibrational dephasing induced by the droplet environment.[38] Fig. 7 shows the time-domain data of the Rb*He exciplex obtained in our experiment. The absolute value of the complex-valued pump–probe transient is shown in (a); recorded (undersampled) quantum beats are enlarged in the inset. The pronounced exaggeration of the ion yield around the zero pump–probe delay (a narrow spike in Fig. 7(a)) is due to the temporal overlap of pump and probe pulses. Outside of this region, a fast decay of the ion yield within 1.5 ps is visible (a shoulder in Fig. 7(a)) which is in accordance with the observed dynamics in ref. 5. In order to make the time evolution of the most prominent spectral features directly accessible, a spectrogram representation of the time domain data obtained by short-time Fourier

analysis (Gaussian window function of 4 ps FWHM, 0.5 ps step size) is shown in Fig. 7(b). The short-time Fourier transform results, however, in a temporal blurring. Thus the discussed fast decay is not observable in Fig. 7(b) but several beat features originating from closely spaced spectral lines are well resolved. Traces along these beats indicate a slow relaxation presumably on the ns timescale (not shown), which is in accordance with the results of ref. 38. However, a longer time window is needed to provide a reliable interpretation in our data.

5.2 Comparison with theory

Despite the availability of more recent *ab initio* PECs of the Rb*He exciplex,[61–63] we compare our data with the semi-empirical potentials calculated by Pascale,[52] which is currently the only model comprising highly excited electronic states. Pascale's pair potentials have proven to accurately describe the energetic structure of alkali–helium exciplexes in many cases.[38,44,46,51] In particular, the results from recent high resolution zero electron kinetic energy (ZEKE) studies of the NaHe exciplex were in much better accordance with the Pascale PECs than with state-of-the-art *ab initio* calculations.[51] To account for spin–orbit couplings, we apply the procedure described in ref. 46 and 49 to the Pascale PECs. To calculate the WPI spectrum, Frank–Condon factors (FCFs) for transitions between the $1^2\Pi_{3/2}$ lower potential and the $2^2\Pi$, $4^2\Delta$, $6^2\Sigma$ upper PECs are evaluated employing the LEVEL 8.0 code of LeRoy.[64] Transition dipole moments are assumed to be constant. The obtained stick spectra are convoluted with a Gaussian of 0.3 cm^{-1} FWHM to account for the experimental resolution. Furthermore, a systematic blue shift of 4 cm^{-1} is applied, which is a reasonable adjustment for such types of numeric models. The resulting spectrum is shown in Fig. 8 together with the experimental data. We find semi-quantitative agreement between experiment and theory, which is quite astonishing considering the degree of detail revealed in the experimental data and the high experimental resolution, which certainly exceeds the precision of the Pascale PECs. For a comparison of observed spectral lines with individual vibronic transitions, we show separately in five subpanels the calculated transitions from the $1^2\Pi_{3/2}$ intermediate PEC to the individual upper potentials (labeled subpanels in Fig. 8). This allows a more precise interpretation of the exciplex spectrum than was possible in previous studies.[5,38] Obviously, the two clusters of lines at higher frequencies correspond primarily to $0 \leftarrow 0$ transitions and do not reflect the vibrational ladder of the $1^2\Pi_{3/2}$ potential, as has been thought before.

The exciplex spectrum has also been calculated including rotational transitions, which yielded much poorer agreement with the experiment (not shown). Thus, rotational features seem to be missing in our measurement despite the fact that our spectral resolution is sufficiently high to reveal those. We assume that rotations are not observed because of efficient cooling by the He droplet environment. This is in accordance with previous vibronic WPI measurements of Rb dimers formed on the surface of He droplets, which also lacked spectroscopic signatures of rotational transitions.[42]
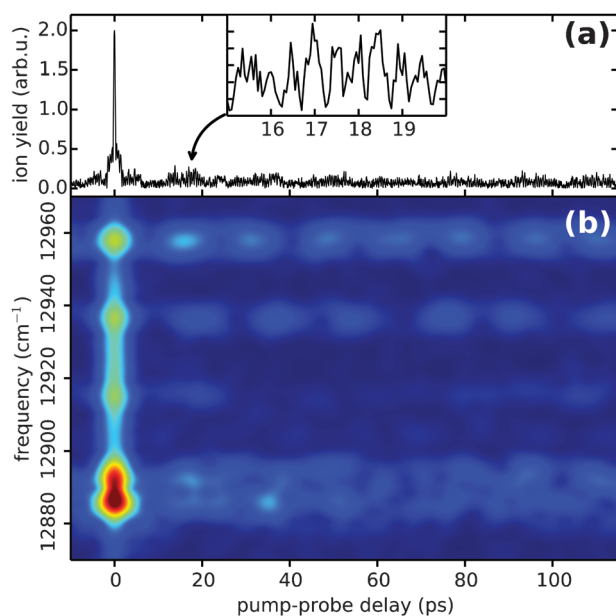

Fig. 7 Time-domain data of the Rb*He exciplex (a) and spectrogram representation obtained by short-time Fourier analysis (b). In the spectrogram, the time evolution of the most prominent spectral features is directly visible.
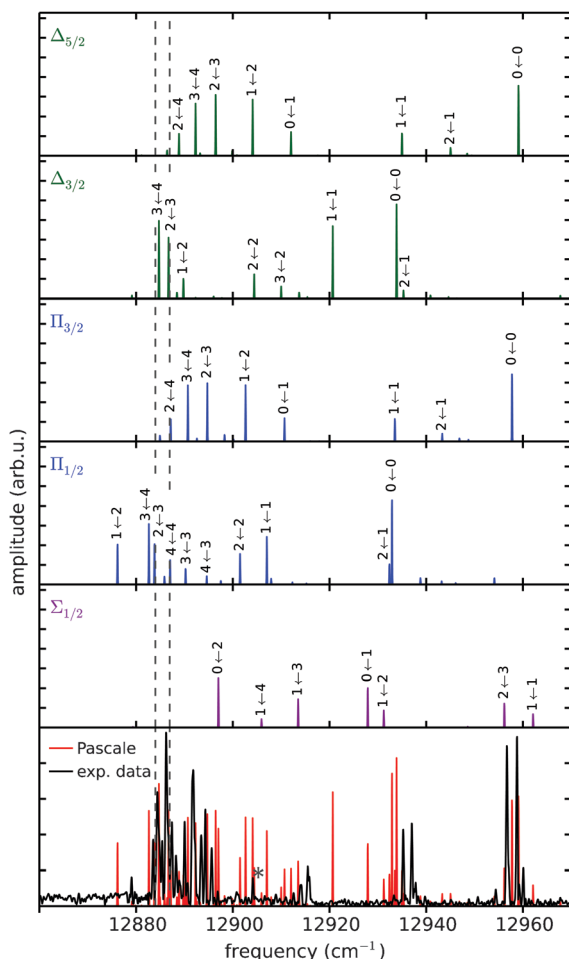
23882 | *Phys. Chem. Chem. Phys.*, 2015, **17**, 23877–23885

This journal is © the Owner Societies 2015

Fig. 8 Experimental Rb*He exciplex spectrum compared with calculations based on the potentials of Pascale.[52] The five upper panels show the calculated FCFs for transitions from the $1^2\Pi_{3/2}$ lower potential separately to each higher-lying potential (label). Adding up all five spectra yields the red spectrum in the bottom panel, which is compared to the experimental data (black). Transitions have been convoluted with a Gaussian of 0.3 cm^{-1} and blue shifted by 4 cm^{-1}. For simplicity only most prominent peaks are labeled.

6 Conclusion

With this work we demonstrate for the first time the applicability of PM-WPI to a molecular sample in the gas phase at very low particle densities. In the WPI experiments performed, electronic coherences were induced in a diatomic molecule allowing us to study the coupled electronic-vibrational dynamics. This is in contrast to pure rovibrational WPI, which is not sensitive to dephasing of electronic coherences but in return demands significantly less phase control. While only few groups have performed electronic WPI on a supersonic beam,[57,65] our work demonstrates for the first time coherent electronic fs spectroscopy of a doped helium droplet beam with sufficient resolution to disentangle congested electronic and vibrational states.

The combination of the PM approach with mass-resolved photoion detection allows us to specifically probe Rb*He

exciplexes formed at the He droplet surface upon laser excitation. We achieve a significant enhancement of the signal-to-noise ratio and an excellent resolution when compared to other experiments on the same system. The WPI data reveals a fully resolved vibrational spectrum for transitions between the $5\Pi_{3/2}$ and the $2^2\Pi$, $4^2\Delta$, $6^2\Sigma$ electronic states. A comparison with a spectrum from the diatomic potentials of Pascale clearly demonstrates that the experimental data are well suited to test fine details of pair interaction potentials. So far for the Rb*He molecule there is no set of potentials available to reproduce the details provided by the experiment and we expect our results to stimulate the development of more accurate potentials.

We note that our experiments provide a new and very promising perspective for applying coherent multidimensional spectroscopy to dilute supersonic beams. Particularly the unique capabilities of synthesizing tailor-made complexes in He droplets combined with two-dimensional spectroscopy could provide new insight into fundamental photophysical and photochemical processes.

Acknowledgements

References

1 M. Fushitani, *Annu. Rep. Prog. Chem., Sect. C: Phys. Chem.*, 2008, **104**, 272–297.
2 K. Ohmori, *Annu. Rev. Phys. Chem.*, 2009, **60**, 487–511.
3 F. Stienkemeier, F. Meier, A. Hägele, H. O. Lutz, E. Schreiber, C. P. Schulz and I. V. Hertel, *Phys. Rev. Lett.*, 1999, **83**, 2320–2323.
4 A. Präkelt, M. Wollenhaupt, C. Sarpe-Tudoran and T. Baumert, *Phys. Rev. A: At., Mol., Opt. Phys.*, 2004, **70**, 063407.
5 M. Mudrich, G. Droppelmann, P. Claas, C. Schulz and F. Stienkemeier, *Phys. Rev. Lett.*, 2008, **100**, 023401.
6 J. Mauritsson, T. Remetter, M. Swoboda, K. Klünder, A. L'Huillier, K. J. Schafer, O. Ghafur, F. Kelkensberg, W. Siu, P. Johnsson, M. J. J. Vrakking, I. Znakovskaya, T. Uphues, S. Zherebtsov, M. F. Kling, F. Lépine, E. Benedetti, F. Ferrari, G. Sansone and M. Nisoli, *Phys. Rev. Lett.*, 2010, **105**, 053001.
7 G. S. Schlau-Cohen, A. Ishizaki and G. R. Fleming, *Chem. Phys.*, 2011, **386**, 1–22.
8 W. P. de Boeij, M. S. Pshenichnikov and D. A. Wiersma, *Chem. Phys. Lett.*, 1995, **238**, 1–8.
9 L. Lepetit, G. Chériaux and M. Joffre, *J. Opt. Soc. Am. B*, 1995, **12**, 2467–2474.

This journal is © the Owner Societies 2015

Phys. Chem. Chem. Phys., 2015, **17**, 23877–23885 | 23883

10 P. Tian, D. Keusters, Y. Suzaki and W. S. Warren, *Science*, 2003, **300**, 1553–1555.

11 T. Brixner, T. Mancal, I. V. Stiopkin and G. R. Fleming, *J. Chem. Phys.*, 2004, **121**, 4221–4236.

12 M. Cowan, J. Ogilvie and R. Miller, *Chem. Phys. Lett.*, 2004, **386**, 184–189.

13 T. Zhang, C. Borca, X. Li and S. Cundiff, *Opt. Express*, 2005, **13**, 7432–7441.

14 C. Li, W. Wagner, M. Ciocca and W. S. Warren, *J. Chem. Phys.*, 2007, **126**, 164307.

15 P. F. Tekavec, G. A. Lott and A. H. Marcus, *J. Chem. Phys.*, 2007, **127**, 214307.

16 A. D. Bristow, D. Karaiskaj, X. Dai, T. Zhang, C. Carlsson, K. R. Hagen, R. Jimenez and S. T. Cundiff, *Rev. Sci. Instrum.*, 2009, **80**, 073108.

17 G. Nardin, T. M. Autry, K. L. Silverman and S. T. Cundiff, *Opt. Express*, 2013, **21**, 28617–28627.

18 D. B. Turner, K. W. Stone, K. Gundogdu and K. A. Nelson, *Rev. Sci. Instrum.*, 2011, **82**, 081301.

19 J. Réhault, M. Maiuri, A. Oriana and G. Cerullo, *Rev. Sci. Instrum.*, 2014, **85**, 123107.

20 J. D. Hybl, A. W. Albrecht, S. M. Gallagher Faeder and D. M. Jonas, *Chem. Phys. Lett.*, 1998, **297**, 307–313.

21 C.-h. Tseng, S. Matsika and T. C. Weinacht, *Opt. Express*, 2009, **17**, 18788–18793.

22 T. Brixner, J. Stenger, H. M. Vaswani, M. Cho, R. E. Blankenship and G. R. Fleming, *Nature*, 2005, **434**, 625–628.

23 A. Nemeth, F. Milota, J. Sperling, D. Abramavicius, S. Mukamel and H. F. Kauffmann, *Chem. Phys. Lett.*, 2009, **469**, 130–134.

24 S. T. Cundiff, *J. Opt. Soc. Am. B*, 2012, **29**, A69–A81.

25 K. J. Karki, J. R. Widom, J. Seibt, I. Moody, M. C. Lonergan, T. Pullerits and A. H. Marcus, *Nat. Commun.*, 2014, **5**, 5869.

26 G. A. Lott, A. Perdomo-Ortiz, J. K. Utterback, J. R. Widom, A. Aspuru-Guzik and A. H. Marcus, *Proc. Natl. Acad. Sci. U. S. A.*, 2011, **108**, 16521–16526.

27 P. F. Tekavec, T. R. Dyke and A. H. Marcus, *J. Chem. Phys.*, 2006, **125**, 194303.

28 J. P. Toennies and A. F. Vilesov, *Angew. Chem., Int. Ed.*, 2004, **43**, 2622.

29 F. Stienkemeier and A. F. Vilesov, *J. Chem. Phys.*, 2001, **115**, 10119–10137.

30 M. Y. Choi, G. E. Douberly, T. M. Falconer, W. K. Lewis, C. M. Lindsay, J. M. Merritt, P. L. Stiles and R. E. Miller, *Int. Rev. Phys. Chem.*, 2006, **25**, 15–75.

31 M. Wewer and F. Stienkemeier, *J. Chem. Phys.*, 2004, **120**, 1239–1244.

32 M. Wewer and F. Stienkemeier, *Phys. Chem. Chem. Phys.*, 2005, **7**, 1171–1175.

33 M. Dvorak, M. Müller, T. Knoblauch, O. Bünermann, A. Rydlo, S. Minniberger, W. Harbich and F. Stienkemeier, *J. Chem. Phys.*, 2012, **137**, 164301.

34 F. Stienkemeier and K. Lehmann, *J. Phys. B: At., Mol. Opt. Phys.*, 2006, **39**, R127.

35 P. Claas, G. Droppelmann, C. P. Schulz, M. Mudrich and F. Stienkemeier, *J. Phys. B: At., Mol. Opt. Phys.*, 2006, **39**, S1151.

36 P. Claas, G. Droppelmann, C. P. Schulz, M. Mudrich and F. Stienkemeier, *J. Phys. Chem. A*, 2007, **111**, 7537.

37 G. Droppelmann, O. Bünermann, C. P. Schulz and F. Stienkemeier, *Phys. Rev. Lett.*, 2004, **93**, 0233402.

38 C. Giese, T. Mullins, B. Grüner, M. Weidemüller, F. Stienkemeier and M. Mudrich, *J. Chem. Phys.*, 2012, **137**, 244307.

39 J. von Vangerow, A. Sieg, F. Stienkemeier, M. Mudrich, A. Leal, D. Mateo, A. Hernando, M. Barranco and M. Pi, *J. Phys. Chem. A*, 2014, **118**, 6604–6614.

40 J. v. Vangerow, O. John, F. Stienkemeier and M. Mudrich, *J. Chem. Phys.*, 2015, **143**, 034302.

41 M. Schlesinger, M. Mudrich, F. Stienkemeier and W. T. Strunz, *Chem. Phys. Lett.*, 2010, **490**, 245–248.

42 B. Grüner, M. Schlesinger, P. Heister, W. T. Strunz, F. Stienkemeier and M. Mudrich, *Phys. Chem. Chem. Phys.*, 2011, **13**, 6816–6826.

43 F. Stienkemeier, W. E. Ernst, J. Higgins and G. Scoles, *J. Chem. Phys.*, 1995, **102**, 615–617.

44 J. Reho, C. Callegari, J. Higgins, W. E. Ernst, K. K. Lehmann and G. Scoles, *Faraday Discuss.*, 1997, **108**, 161–174.

45 C. P. Schulz, P. Claas and F. Stienkemeier, *Phys. Rev. Lett.*, 2001, **87**, 153401.

46 F. R. Brühl, R. A. Trasca and W. E. Ernst, *J. Chem. Phys.*, 2001, **115**, 10220–10224.

47 L. Fechner, B. Grüner, A. Sieg, C. Callegari, F. Ancilotto, F. Stienkemeier and M. Mudrich, *Phys. Chem. Chem. Phys.*, 2012, **14**, 3843.

48 J. Reho, J. Higgins, C. Callegari, K. K. Lehmann and G. Scoles, *J. Chem. Phys.*, 2000, **113**, 9686–9693.

49 J. Reho, J. Higgins, C. Callegari, K. K. Lehmann and G. Scoles, *J. Chem. Phys.*, 2000, **113**, 9694–9701.

50 E. Loginov and M. Drabbels, *J. Phys. Chem. A*, 2007, **111**, 7504–7515.

51 E. Loginov, A. Hernando, J. A. Beswick, N. Halberstadt and M. Drabbels, *J. Phys. Chem. A*, 2015, **119**, 6033–6044.

52 J. Pascale, *Phys. Rev. A: At., Mol., Opt. Phys.*, 1983, **28**, 632–644.

53 E. Loginov and M. Drabbels, *J. Phys. Chem. A*, 2014, **118**, 2738–2748.

54 L. D. Noordam, D. I. Duncan and T. F. Gallagher, *Phys. Rev. A: At., Mol., Opt. Phys.*, 1992, **45**, 4734–4737.

55 J. Christian, B. Broers, J. Hoogenraad, W. van der Zande and L. Noordam, *Opt. Commun.*, 1993, **103**, 79–84.

56 M. Bellini, A. Bartoli and T. W. Hänsch, *Opt. Lett.*, 1997, **22**, 540–542.

57 V. Blanchet, C. Nicole, M.-A. Bouchene and B. Girard, *Phys. Rev. Lett.*, 1997, **78**, 2716–2719.

58 S. Mukamel, *Principles of nonlinear optical spectroscopy*, Oxford University Press, 1995.

59 N. F. Scherer, R. J. Carlson, A. Matro, M. Du, A. J. Ruggiero, V. Romero-Rochin, J. A. Cina, G. R. Fleming and S. A. Rice, *J. Chem. Phys.*, 1991, **95**, 1487–1511.

23884 | *Phys. Chem. Chem. Phys.*, 2015, **17**, 23877–23885

This journal is © the Owner Societies 2015

60 P. Heister, M. Mudrich, 2008, unpublished material.

61 L. Blank, D. E. Weeks and G. S. Kedziora, *J. Chem. Phys.*, 2012, **136**, 124315.

62 A. Chattopadhyay, *J. Phys. B: At., Mol. Opt. Phys.*, 2012, **45**, 035101.

63 F. Bouhadjar, K. Alioua, M. T. Bouazza and M. Bouledroua, *J. Phys. B: At., Mol. Opt. Phys.*, 2014, **47**, 185201.

64 J. R. LeRoy, *LEVEL 8.0: A Computer Program for Solving the Radial Schrödinger Equation for Bound and Quasibound Levels*, University of Waterloo Chemical Physics Research Report CP-663, 2007.

65 K. Ohmori, H. Katsuki, H. Chiba, M. Honda, Y. Hagihara, K. Fujiwara, Y. Sato and K. Ueda, *Phys. Rev. Lett.*, 2006, **96**, 093002.

This journal is © the Owner Societies 2015

Phys. Chem. Chem. Phys., 2015, **17**, 23877–23885 | **23885**